High fidelity sky coverage analysis via time domain adaptive optics simulations

Lianqi Wang,[1,*] Brent Ellerbroek,[1] and Jean Pierre Veran[2]

[1]TMT Observatory Corporation, 2632 East Washington Boulevard, Pasadena, California 91107, USA

[2]Herzberg Institute of Astrophysics, 5071 West Saanich Road Victoria, British Columbia V9E 2E7, Canada

*Corresponding author: lianqiw@tmt.org

Received 3 June 2009; revised 20 July 2009; accepted 18 August 2009;
posted 20 August 2009 (Doc. ID 112301); published 10 September 2009

We describe a high fidelity simulation method for estimating the sky coverage of multiconjugate adaptive optics systems; this method is based upon the split tomography control architecture, and employs an AO simulation postprocessing technique to evaluate system performance with hundreds of randomly generated natural guide star (NGS) asterisms. A novel technique to model the impact of quadratic wavefront aberrations upon the NGS point spread functions is described; this is used to model the variations in system performance with different asterisms, and is crucial for obtaining accurate results with the postprocessing technique. Several design and algorithm improvements help to reduce the residual wavefront error in the tip/tilt and plate scale modes that are controlled using the NGS asterism. These improvements include choosing the right wavefront sensor (WFS) pixel size, optimal pixel weights, and type II control of the plate scale modes. © 2009 Optical Society of America

OCIS codes: 010.1080, 010.7350.

1. Introduction

Current [1–3] and next generation [4,5] ground based astronomical telescopes rely upon laser guide star adaptive optics (LGS AO) systems to achieve diffraction limited resolution. Because the laser is launched from the ground and reflected back from the sodium layer, it cannot reliably measure the tip/tilt wavefront aberration caused by the atmospheric turbulence or telescope vibration. Therefore most LGS AO systems also use one or several low order natural guide star (NGS) wavefront sensors (WFSs) to provide tip/tilt wavefront measurements.

For a multiconjugate or multiobject adaptive optics system with a nonnegligible field of view, multiple NGS WFSs are needed to provide measurements of both global tip/tilt and tilt anisoplanatism (i.e., field varying tip/tilt). The sky coverage of an AO system describes the probability of finding natural guide stars within the NGS patrol field that are bright enough to enable the system to achieve its performance requirements.

High fidelity simulations of multiconjugate adaptive optics (MCAO) systems are time consuming, but rigorous sky coverage estimates must be based upon simulations performed with a large number of randomly generated NGS asterisms. Previous sky coverage analyses of LGS MCAO and multiobject adaptive optics (MOAO) systems [6,7] have therefore employed much simplified simulation tools based upon (1) linear, low order, Zernike-based models of wavefront sensing and correction on an ideal circular pupil, (2) an idealized linear model of the high-order LGS wavefront control loop with zero time delay, no LGS WFS measurement noise, and no LGS pointing jitter, and (3) a simplified, time-averaged model for the degree of NGS "sharpening" provided by the higher-order LGS adaptive optics as a function of the NGS location in the AO system field of view. The above approach provides a detailed analysis of some, but not all, of the potential tip/tilt error sources that must be considered when evaluating sky coverage. In particular, the residual errors due to tilt

0003-6935/09/275076-12$15.00/0

anisoplanatism, servo lag, and telescope wind shake can be calculated using these tools. But evaluating the tip/tilt errors due to other important effects including NGS WFS measurement noise, time-varying aberrations of the partially compensated NGS point spread function (PSF), and undersampling of the NGS PSF by the NGS WFS detector requires more rigorous simulation models. These include physical optics modeling of the NGS WFS and a simulation of the higher-order LGS control loop.

In this paper, we describe a high fidelity, time domain simulation for a complete NGS/LGS MCAO control architecture, which can be used to address all these limitations of the previous sky coverage analysis. This physical optics sky coverage simulation concept was first described in a previous report [8]. We have now implemented this in software and tested it.

Section 2 reviews the overall hardware and control system parameters for the narrow field infrared AO system (NFIRAOS), the specific LGS MCAO system that has motivated the development of this sky coverage modeling technique. Section 3 reviews the basic theory behind the approach. Section 4 summaries the system and atmospheric parameters for sky coverage simulation. Section 5 describes several control algorithm refinements and parameter trade studies found to be useful in improving sky coverage for NFIRAOS. Section 6 outlines the sky coverage results for NFIRAOS and tabulates the NFIRAOS tip/tilt and plate scale error budgets at median sky coverage. A summary and a discussion of possible future work are given in Section 7.

2. NFIRAOS LGS MCAO System and "Split Tomography" Control

The Thirty Meter Telescope (TMT) narrow field infrared adaptive optics system (NFIRAOS) [4] is an MCAO system with two deformable mirrors (DMs) conjugated to the range of 0.0 and 11.3 km, respectively, an asterism of 6 sodium laser guide stars arranged in a pentagon with a 35″ radius plus one more on axis, and up to three natural guide star low-order wavefront sensors (1 tip/tilt/focus/astigmatism (TTF) and up to two tip/tilts only). The ground-conjugate DM is mounted on a tip/tilt stage (TTS) to eliminate the need for a separate tip/tilt mirror. Due to the lower bandwidth of this TTS (we measured 90 Hz on the TTS prototype made by CILAS), a woofer/tweeter type II control law is implemented that uses the TTS to compensate the low temporal frequency, high stroke tip/tilt wavefront errors, and the DM to control the high temporal frequency, but low stroke tip/tilt errors [9].

The performance requirements for NFIRAOS include diffraction-limited turbulence compensation over fields of view (FOVs) of up to 30″ in diameter. The patrol field for the low-order NGS WFS is a larger, nonvignetted, 2′ diameter circular FOV. The NGSs are acquired via probe arms that patrol outside of the science FoV. The NGS WFS will operate in the near infrared (J and H bands) since (1) the NGS images will be partially "sharpened" by the NFIRAOS system, and (2) more guide stars are available in the near infrared. The K band is excluded because the selected detector (Hawaii-1RG) has negligible quantum efficiency at this wavelength. The WFS pixel size will be matched to the diffraction limited image size to improve the signal to noise ratio (SNR) and sky coverage. The NGS has a limiting magnitude of 22, above which the SNR will be too low in our sampling frequency range (10–800 Hz).

The split tomography control algorithms [10] will be used in these sky coverage coverage simulations and also in the actual real-time control hardware for NFIRAOS. In split tomography, the separate LGS and NGS control loops are driven independently, as illustrated in Fig. 1(a). The atmospheric tomography step of the LGS control loop applies a minimum variance estimator to tip/tilt removed, pseudo open loop LGS WFS gradients. Each LGS position is stabilized by a separate uplink fast steering mirror in the laser launch telescope to ensure that the LGS WFS has sufficient linear dynamic range. The residual uplink jitter is of the order of 50 milliarcseconds (mas) RMS. The NGS control loop uses a

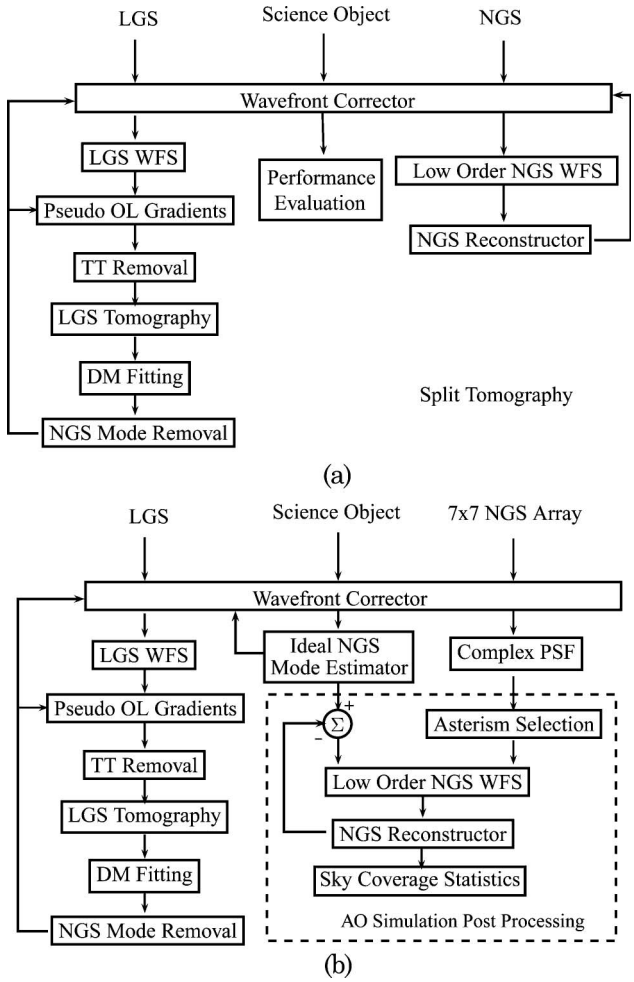

Fig. 1. (Color online) Split tomography control architecture of NFIRAOS and the associated sky coverage analysis approach.

noise-weighted, least square reconstructor and can operate at a different frame rate than the LGS loop depending upon the brightness of the NGS. The separation between the LGS and NGS loops is improved by nulling the component of the LGS-controlled DM commands that lies in the span of the NGS-controlled modes. This component is nonzero on account of the noise in the LGS measurements and the use of a minimal variance estimator. We will focus on the control of the NGS modes in this paper.

The NGS controlled modes are defined as the tip/tilt and (largely) tilt anisoplanatism modes that produce pure tip/tilt in each LGS wavefront, and are therefore not sensed by the three tilt-removed LGS WFSs. Most of the error in the tilt anisoplanatism modes can be corrected by applying a combination of three quadratic Zernike modes with proportional amplitudes in two conjugate planes [11]. For a two DM MCAO system like the TMT NFIRAOS, the following equations describe the global tip/tilt modes (m_1 and m_2) and these three dominant tilt anisoplanatism modes (m_3 to m_5) that must be measured using the low order NGS WFS:

$$\begin{aligned} m_1 &= (x_0; 0), \\ m_2 &= (y_0; 0), \\ m_3 &= ([x_0^2 + y_0^2]; -[x_1^2 + y_1^2]/s_c^2), \\ m_4 &= ([x_0^2 - y_0^2]; -[x_1^2 - y_1^2]/s_c^2), \\ m_5 &= ([x_0 y_0]; -[x_1 y_1]/s_c^2), \\ M &= (m_1|m_2|m_3|m_4|m_5), \end{aligned} \tag{1}$$

where x_0, y_0 and x_1, y_1 are the actuator coordinates on the ground and upper DMs. The coefficient $s_c = 1 - h_c/h_s$ is the cone effect for a DM conjugated to range h_c and an LGS at range h_s. The global tip/tilt mode vectors m_1 and m_2 have the tip/tilt Zernike modes applied to the ground DM only. The tilt anisoplanatism mode vectors m_3 to m_5 each contain a quadratic Zernike mode with proportional amplitudes on the ground and upper DMs, whose combined effect produces pure tip/tilt in the LGS wavefront sensors (thus not sensed), but contains field dependent tip/tilt (plate scale effect) and quadratic wavefront aberrations across the science field and NGS patrol field. These tilt anisoplanatism errors are therefore named plate scale modes. The NGS mode M is a five-column model matrix composed of the five mode vectors m_1 to m_5. It is worth pointing out that these plate scale modes arise solely from the fact that the LGS is propagated from a finite altitude, while the NGS and science are from infinity.

Detailed formulation of the split tomography approach can be found in [10]. We summarize the measurement and control of the NGS modes based upon the NGS WFS measurements here:

$$a = P_L a_L + a_N, \tag{2}$$

$$s_N = G_N[H_x^N x - H_a^N a], \tag{3}$$

$$\delta a_N = M G_M^{\dagger} s_N. \tag{4}$$

Here a_L and a_N are the DM actuator commands computed from the LGS tomography and NGS measurements, a is the total DM command, P_L is the NGS mode removal operator for the LGS DM commands, x is the atmospheric turbulence optical path difference (OPD) defined on planes conjugated to several (six in our case) different altitudes, H_x^N and H_a^N are interpolation operators for the influence of the turbulence OPD and DM actuators on the rays (in 1/64 m sampling) traced from the NGS to the aperture plane, G_N is the NGS WFS gradient operator that computes the average gradient of the turbulence OPD (in geometrical simulations) or the center of gravity for the images formed (in physical optics simulations) in each of the subapertures, the NGS mode matrix M represents the NGS modes in terms of DM actuator commands, $G_M = G_N H_a^N M$, a five-column matrix is the influence matrix from the five NGS modes onto NGS WFS measurements, and finally δa_N is the estimate of the residual closed-loop error in the NGS modes that is added into a_N after servo filtering. The NGS modal reconstructor $G_M^{\dagger}$ implements a least square estimation weighted by the NGS measurement noise, and is computed using

$$\hat{a} = \arg\min \|G_M a - s^N\|_{C_N^{-1}} = G_M^{\dagger} s^N, \tag{5}$$

$$G_M^{\dagger} = (G_M^T C_N^{-1} G_M)^{-1} G_M^T C_N^{-1}, \tag{6}$$

where C_N^{-1} is the inverse of the NGS measurement error covariance matrix.

The projection matrix P_L is used to minimize the cross coupling between the LGS and NGS measurements. In the original split-tomography approach, P_L was chosen so that the NGS WFS gradient generated by $P_L a_L$ will not be reconstructed into any NGS mode, i.e.,

$$G_M^{\dagger} G_N H_a^N P_L a_L = 0 \tag{7}$$

for arbitrary a_L. Notice that $G_M^{\dagger} G_N H_a^N = M^{\dagger}$ is the pseudo inverse of M, $M^{\dagger} = (M^T W_g M)^{-1} M^T W_g$, with weighting $W_g = H_a^{NT} G_N^T C_N^{-1} G_N H_a^N$. It is straightforward to confirm that Eq. (7) is satisfied with $P_L = I - MM^{\dagger}$. Notice that $G_M^{\dagger}$ and C_N^{-1}, and consequently P_L, then depend upon the choice of NGS asterism.

The split tomography architecture has several practical advantages over the traditional integrated tomography approach that operates on concatenated measurements of both LGS and NGS WFS [12]: (1) The formulation of split tomography for only tip/tilt removed LGS WFS measurements has less complexity than for concatenated LGS/NGS measurements, and thus simpler iterative solutions can be used with fewer iterations; (2) the NGS loop can be controlled

using a direct least square solution; (3) the NGS control loop generally runs at a slower rate than the LGS control loop due to limited brightness of available NGSs, and it is simpler to implement separate temporal control of the LGS and NGS modes in the split tomography architecture, and finally (4) sky coverage analysis using efficient postprocessing techniques is feasible thanks to the separated control of the LGS and NGS loops.

3. Approach to Sky Coverage Analysis for "Split Tomography" Control

The NFIRAOS split tomography control architecture described in Section 2 enables the efficient modeling and evaluation of the LGS and NGS control loops as a two step process. The first step is a simulation of the high-order LGS control loop using our Linear Adaptive Optics Simulator (LAOS) code [13]. During this step, the five NGS-controlled modes contained in the atmosphere are corrected perfectly, without the degrading effects of WFS noise or servo delay, to minimize the wavefront error over the science FoV. A time history of the resulting NGS WFS PSFs, the best fit of NGS modes, and the associated geometric gradient measurements are recorded for an array of both TT and TTF WFSs positioned at 29 NGS locations arranged on a grid with a spacing of 20″ across the NFIRAOS 2′ FoV, as shown in Fig. 2.

During the postprocessing step, for each random NGS asterism, we will replay the movie of the higher order loop and estimate the actual correction to the NGS modes from the NGS measurements, which is computed from the saved NGS WFS PSFs (in physical optics simulations) or geometric gradient measurements (in geometric simulations), and the best-fit NGS modes.

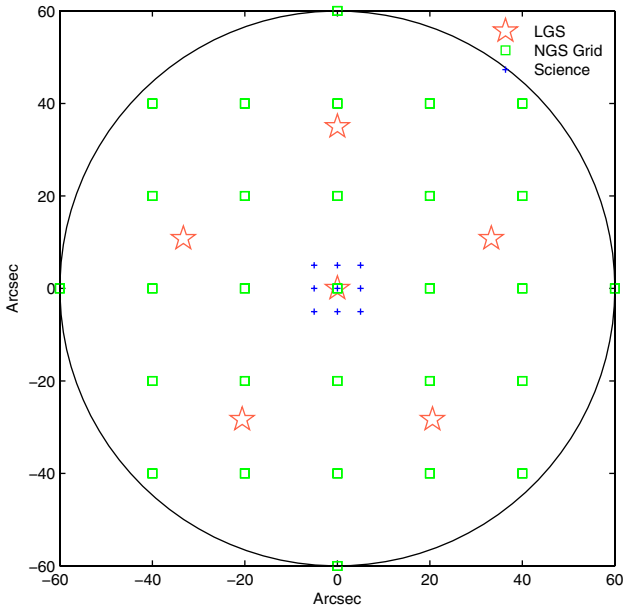

Fig. 2. (Color online) Sketch of the LGS asterism (orange stars, on a circle of 35″ radius), NGS grid (green squares) and 10″ science field (blue pluses) for the sky coverage analysis of NFIRAOS.

Accurate sky coverage estimates require the simulation of hundreds of NGS asterisms, and we must break the dependence between the LGS and NGS WFS measurements in Eqs. (2)–(4) so that we can estimate the performance of the NGS loop without rerunning the full simulation of LGS tomography. We change the order of computation by first applying an ideal correction of the NGS modes during the higher order LGS simulation,

$$m^* = (H_a^{sc}M)^{\dagger}(H_x^{sc}x - H_a^{sc}P'_L a_L), \tag{8}$$

$$(H_a^{sc}M)^{\dagger} = (M^T H_a^{scT} W_a H_a^{sc} M)^{-1} M^T H_a^{scT} W_a, \tag{9}$$

$$a^* = P'_L a_L + M m^*, \tag{10}$$

$$s_N^* = G_N[H_x^N x - H_a^N a^*], \tag{11}$$

where H_x^{sc} and H_a^{sc} are interpolation operators for the influence of the turbulence OPD and DM actuators on the rays (in 1/64 m sampling) traced from the science objects (3×3 in a $10'' \times 10''$ square FoV with Simpson weighting in our case) to the aperture plane. $(H_a^{sc}M)^{\dagger}$ is the least square reconstructor to compute the best fit of the NGS modes onto the residual OPDs in the science field, for the diagonal weighting matrix W_a composed of the aperture amplitude function. The optimal fit NGS mode correction m^* is then added to the NGS mode removed LGS DM actuator command without servo filtering to obtain the total DM command a^*, which is applied during the higher order closed loop simulation. The NGS measurement s_N^* with ideal NGS mode correction applied is saved for geometric simulations during the postprocessing step.

We have changed P_L in Eq. (2) to P'_L in Eq. (8) for efficient postprocessing, since P_L cannot be constructed simultaneously for multiple asterisms with individual values for G_M and C_N^{-1}. We choose to orthogonalize the influence of the LGS and NGS mode wavefront errors in the science field by imposing $(H_a^{sc}M)^{\dagger}H_a^{sc}P'_L a_L = 0$, which gives $P'_L = I - M(H_a^{sc}M)^{\dagger}H_a^{sc}$. The consequence is that the DM actuator commands generated from the LGS control loops now potentially couple into the NGS WFS measurements, although they remain orthogonal to the NGS modes on the science field. Simulations for sample asterisms show that this modification degrades NGS loop performance only marginally.

The NGS control loop performance can now be simulated and evaluated in postprocessing for an arbitrary asterism. Let m be the actual NGS modes (a five-element vector) applied at certain time step for a given asterism; the closed loop correction δm is then

$$\delta m = G_M^{\dagger}(s_N^* + G_M(m^* - m) + n), \tag{12}$$

in geometric simulation or

$$\delta m = G_M^{\dagger} CoG(I(\theta; m^* - m) + n) \qquad (13)$$

in physical optics simulations, where we use Fourier optics techniques to compute NGS PSFs, sample them onto detector pixels to obtain $I(\theta, m^* - m)$ (where θ denotes NGS direction), and finally apply a centroiding method (using either center of gravity or matched filter algorithm as described Subsection 5.E) to obtain the NGS WFS measurement. The term n denotes various error sources (e.g., photon and detector read noise). Subsection 5.A further describes the method to obtain the detector reading $I(\theta, m^* - m)$. The closed loop correction δm is then added to m after servo filtering as described in Subsection 5.B and 5.C.

4. Sky Coverage Simulation Parameters and Methods

The NFIRAOS system was described in Section 2. The nominal sky coverage simulations are carried out for median seeing conditions at the Galactic Pole, which represents the worse case for sky coverage. The six-layer turbulence profile typical of Cerro Pachon [14], as shown in Table 1, is used for the simulation. The Besancon star count model [15,16] can be used to generate random star catalogs for any direction in the sky. The model catalogs include visible and near-infrared magnitudes for each star. This model is based on theoretical model of the Galaxy and is the best model available to our knowledge that includes near-infrared star magnitudes. We have compared the star densities obtained with the Besancon model with J and K-band star counts in four high Galactic latitude fields from the Canada France Hawaii Telescope (CFHT) Legacy Survey (Willott, [17]) and we have found overall consistency between them down to magnitude $J = 21$ and $K = 20$ (Andersen [18]). The binary fraction at high Galactic Latitude is expected to be low, so our assumption that the stars are randomly distributed in the field should not greatly affect the sky coverage of NFIRAOS. The $1k \times 1k$ Teledyne Hawaii-1RG near infrared detector with $5e^-$ readout noise is chosen as the baseline. Table 2 summarizes the system and atmospheric parameters.

During the sky coverage simulation, 500 different random star fields are generated from the Besancon star count model. For each star field, the Zernike based geometric sky coverage simulator [7] is called to preselect a three-star asterism that gives the best performance (it takes too much computation time to evaluate all possible combinations via the time domain postprocessing technique). The postprocessing described in Section 3 then evaluates the optimal NGS sampling frequency and obtains the minimum wavefront error in addition to the error due to noise and turbulence. The telescope wind shake error is computed for each NGS sampling frequency using the wind shake power spectrum density and the servo rejection function of the tip/tilt loop. The residual wind shake error ranges from 5 to 30 nm RMS for typical sampling frequencies for an input of 20 mas RMS jitter at 75 percentile wind conditions. For TMT, 1 mas RMS tip/tilt jitter is equivalent to about 36 nm RMS wavefront error. Finally, the sodium tracking error [19] is obtained from a lookup table for each NGS sampling frequency, based upon the expected variability of the range to the sodium layer. The sodium tracking error ranges from 6 to 21 nm RMS at high and low sampling frequencies. The wind shake and sodium tracking error are not dominant terms. The sky coverage cumulative distribution function is then obtained by sorting the results for the 500 star fields.

Table 1. Six-Layer Turbulence Profile Typical of Cerro Pachon[a]

Layer i	h_i (m)	γ_i	v_i (m/s)
1	0	0.6523	5
2	2577	0.1723	13
3	5155	0.0551	20
4	7732	0.0248	30
5	12887	0.0736	20
6	15464	0.0219	10

[a]The height h_i, relative turbulence strength γ_i, and wind speed v_i are shown for each layer i.

5. Simulation Upgrades and Trade Studies

Several simulation upgrades and trade studies have been performed to obtain accurate and optimal results using this basic simulation approach. These include the following:

1. For physical optics simulations, the impact of the residual NGS modes $m^* - m$ upon the NGS PSF and the NGS WFS measurement s_N is implemented by applying both the tip/tilt and quadratic components of the residual NGS modes and then recomputing the PSF, instead of simply shifting the PSF by the tip/tilt component. This is necessary for accurate results, since the impact of the quadratic wavefront aberrations is nontrivial.
2. Type II control of the plate scale modes, and improved type II control of tip/tilt (to account for the measured 90 Hz response of the actual TTS hardware) have been implemented to reduce the error due to servo lag.
3. Adaptively "demoting" the TTF WFS to simulate a TT WFS for those asterisms where this improves performance.
4. The WFS pixel size has been adjusted to contain the full core of the diffraction limited PSF and to improve the SNR, since detector read noise is nonnegligible.
5. For physical optics simulations, the classical matched filter [20] for estimating the motion of the NGS images outperforms the constrained matched filter previously developed for LGS WFS applications [21], primarily on account of the amplified sensitivity to noise of the constrained matched filter when used with subpixel images.

Table 2. System and Atmospheric Parameters

Parameter	Value
Telescope diameter (D)	30 m
Turbulence outer scale	30 m
Fried's parameter (median seeing)	0.15 cm at 0.5 μm
Fried's parameter (25% seeing)	0.25 cm at 0.5 μm
Telescope wind shake (75th percentile)	20 mas
Mean height of sodium LGS (h_s)	90 km
DM conjugate altitudes (h_c)	0, 11.3 km
AO order of correction	60 × 60
End-to-end optical throughput	0.4
Detector passband	J and H bands (1.25 and 1.65 μm)
Detector pixel size	λ_H/D
Detector pixel count	1024 × 1024 during acquisition ~4 × 4 in closed loop run
Detector quantum efficiency	0.8 in both J and H bands
Detector readout noise	5e^-/pixel/read
Detector dark current	0
Sky background (J band)	16.25 magnitude/arc sec^2
Sky background (H band)	14.40 magnitude/arc sec^2
Intensity of zero magnitude star (J band)[23]	3.77×10^9 photons/m^2/s
Intensity of zero magnitude star (H band)[23]	3.17×10^9 photons/m^2/s
NGS limiting magnitude	22
Number of TTF WFS (2 × 2 subapertures)	1
Number of TT WFS (single subaperture)	2
Science FoV	10″ × 10″ square
NGS patrol field FoV	2′ diameter circular FoV outside of science FoV

Several of these modifications are described further in the following subsections.

A. PSF Modeling

In physical optics simulations, the gradient operators are no longer linear, and we need to estimate the gradients from the simulated NGS detector readings to correctly model the effects of detector noise and WFS nonlinearity. The NGS-controlled modes are optimally corrected during the LAOS simulation, and we need to add the residual errors back into the saved NGS PSFs during the postprocessing step for each NGS asterism. In our original approach, the PSFs were simply shifted according to the residual tip/tilt wavefront error. This approach turned out to be seriously inaccurate when we compared the NGS images computed in the postprocessing step with the results of integrated LAOS simulations. The wavefront error is underestimated by about 30 nm RMS for a typical asterism, and more for poor cases.

Our solution to this problem is to store the central core of the complex PSF, which is the Fourier transform of the complex pupil function, without computing its modulus squared to form the final PSF. We can recover a coarsely sampled version of the original complex pupil function in postprocessing by an inverse Fourier transform of the complex PSF core. Since the NGS plate scale (quadratic) modes are very smooth functions, we can alter the coarsely sampled wavefront via multiplication with the phase distortion caused by these modes:

$$A(r;m) = \mathcal{F}^{-1}[\mathcal{F}[A(r;m^*)]](r)e^{-ikM(r)(m-m^*)}, \quad (14)$$

$$\mathrm{PSF}(\theta;m) = \|\mathcal{F}[A(r;m)](\theta)\|^2, \quad (15)$$

where m^* is the ideal NGS mode correction made during the first step of the sky coverage simulation, $A(r;m^*)$ is the corresponding complex pupil function, and m is the residual NGS modes for each simulated asterism obtained during the postprocessing step. The PSFs are then sampled on the detector pixels to form detector output (only center 8 × 8 pixels are simulated). This model turns out to agree well with integrated simulations, with some modest errors remaining due to the coarse sampling of the pupil function. Figure 3 shows a comparison of a typical NGS PSF computed using the two methods with a large amount of residual plate scale mode to highlight the difference.

B. Plate Scale Mode Control Law

A type II controller with a lead filter has been constructed to obtain improved error rejection of the plate scale modes for faint NGS with low WFS sampling frequencies. The type II controller is composed of two simple integrators in series, combined with a lead filter to create enough phase margin near the crossover frequency. The transfer function of the type II controller, as expressed in Laplacian domain, is given by

$$H(s) = gH_{\mathrm{int}}(s)H_{\mathrm{int}}(s)H_{\mathrm{lead}}(s), \quad (16)$$

where

$$H_{\mathrm{lead}}(s) = \frac{1+Ts}{1+aTs}, \quad (17)$$

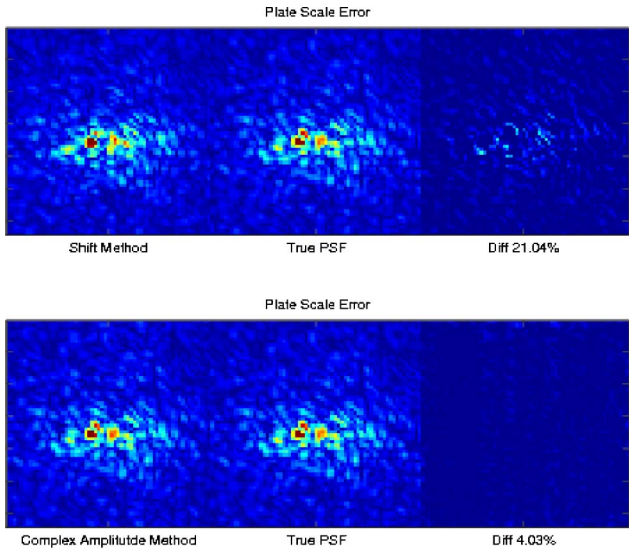

Fig. 3. (Color online) Comparison of the two methods to implement the influence of residual NGS modes on the NGS WFS PSF. A large amount of the first plate scale mode (mode 3, following tip/tilt) is used to indicate the difference. The top panel illustrates the error introduced by simply shifting the PSF, and the bottom panel includes the effects of the wavefront distortions caused by the quadratic modes.

$$H_{\text{int}}(s) = \left(\frac{z}{z-1}\right)_{z=e^{T_s s}} = \frac{1}{1-e^{-T_s s}}, \qquad (18)$$

and g is the overall gain factor. The lead filter $H_{\text{lead}}(s)$ has a positive phase peak of $\theta = \arctan(1+a)/(2\sqrt{a})$ near $f = 1/\sqrt{4\pi^2 a T^2}$ or $s = i2\pi f$.

The parameters a, T, and overall gain g need to be optimized to maximize the error rejection and minimize the noise propagation as a function of the WFS sampling frequency. The optimization process is carried out by first determining the crossover frequency and phase lead needed for 45° phase margin (of the open loop transfer function) without the lead filter. Then the parameter a is determined from the phase lead, and T is determined by setting f to the crossover frequency. Finally, the total loop gain g is optimized by balancing the error rejection against noise propagation. For a low sampling frequency with a good SNR, g is determined by limiting the noise amplification to 1 to prevent the gain from becoming too large, which still gives reasonably good rejection. At a high sampling frequency with a low SNR, g is determined by minimizing the total residual error due to noise and servo lag.

Figure 4 shows the PSDs used for optimization (left panel), and the optimized servo coefficients (right panel) as a function of sampling frequency for a typical asterism (solid curves), and the coefficients obtained by simply limiting the noise amplification to 1 (dashed curves). The total loop gain g is significantly reduced at high bandwidth in order to minimize the total residual error.

Figure 5 compares the performance achieved with the new type II control law against the original approach, which utilized woofer/tweeter type II control [22] for tip/tilt and simple integrator control for the place scale modes. In the top panel, the total residual wavefront errors (WVE) in the five NGS modes are shown as a function of the WFS sampling frequency for a typical asterism. We can see that the type II integrator (solid lines) has better error rejection for the plate scale modes toward lower sampling frequencies and that the reduction of the gain also reduces the error at high sampling frequencies. The bottom panel shows the reduction (in quadrature) of the residual wavefront error in the tip/tilt modes and a complete set of NGS modes as a function of the sky coverage. The wind shake and sodium tracking errors are also included, which limits how low the sampling frequency can be set because the wind shake PSD

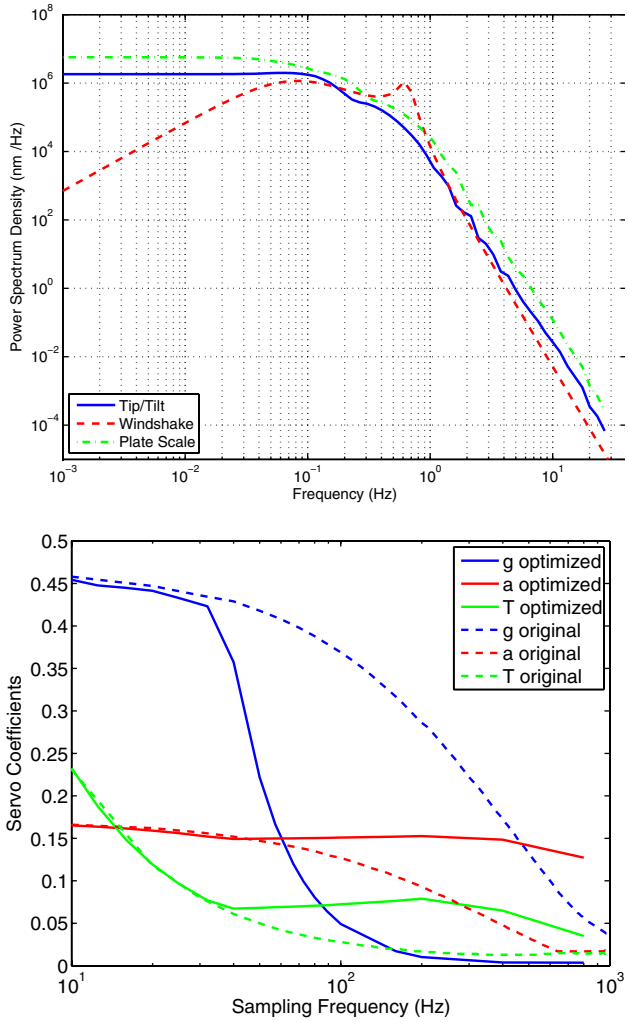

Fig. 4. (Color online) Top panel: The PSDs of the atmospheric plate scale modes that are used for the servo optimization. The PSDs of the atmospheric tip/tilt and telescope wind shake are also used for the servo optimization of the tip/tilt control loops, as described in Subsection 5.C. Bottom panel: Sample servo coefficients. The dashed curves show the original coefficients optimized by always setting noise amplification to 1. The solid curves show the reoptimized coefficients for a typical asterism to limit the noise propagation at high bandwidth. The total loop gain g is significantly reduced at high bandwidth due to the low SNR in this case.

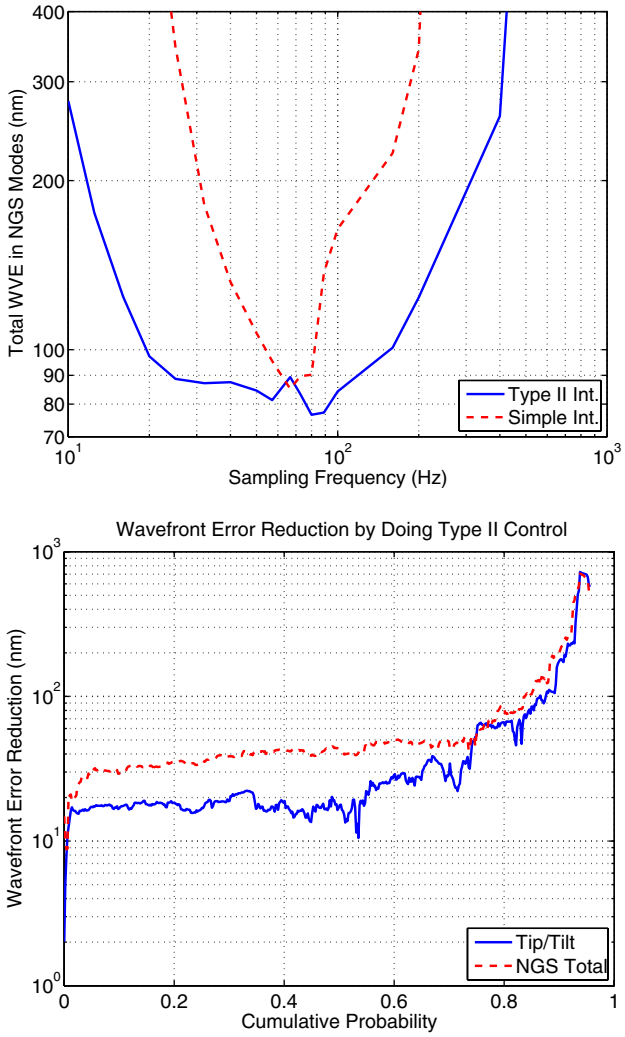

Fig. 5. (Color online) Wavefront error of reoptimized type II control is reduced in comparison with simple integrator control. The top panel shows the wavefront error in the full set of NGS modes as a function of the sampling frequency for a typical asterism. The bottom panel shows the wavefront error reduction (in quadrature) of the type II control compared against the original approach as a function of sky coverage.

has nonnegligible high frequency content. Nevertheless, the gain from the new type II controller is still significant.

C. Tip/Tilt Control and Residual Tip/Tilt Wind Shake Error

We have developed an improved type II woofer/tweeter controller with a lead filter to optimize tip/tilt compensation using the TTS and DM. This type II controller is similar to the one used for the plate scale modes, albeit optimized with a different disturbance PSD (as shown in Fig. 4). The output of the controller is split between the woofer (TTS) and the tweeter (DM surface) by applying a low and a high pass filter (with a 20 Hz cutoff frequency in this case) that sum to 1.

The wind shake error rejection obtained by this method is illustrated in Fig. 6. The residual wind shake error obtained with the new servo coefficients

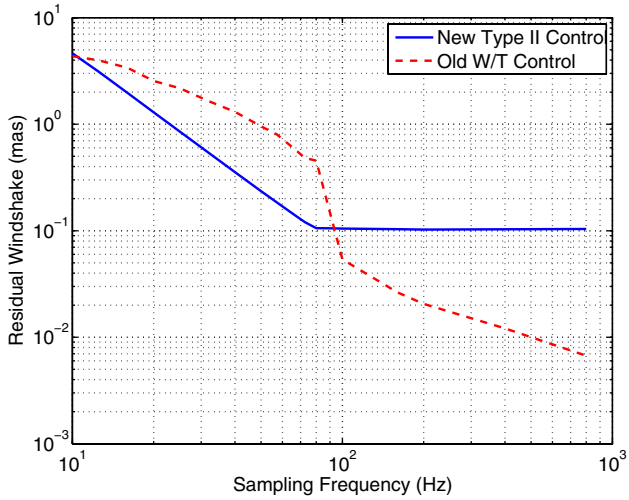

Fig. 6. (Color online) Comparison of residual wind shake using the new type II controller and the old woofer/tweeter control law.

is much reduced at sampling frequencies between 10 and 100 Hz. The leveling off of performance above 100 Hz is due to the reduced gain used to reduce the noise propagation.

D. Detector Pixel Size

NFIRAOS will use the J and H spectral bands for low-order NGS wavefront sensing to maximize the sky coverage. In the original design, the TT and TTF WFS used diffraction-limited sampling of the J band PSF with a detector pixel size of λ_J/d, where λ_J is the wavelength in the J band and d is the subaperture diameter. It was found that performance can be modestly improved by enlarging the detector pixel size to λ_H/d, to fully contain the core of the H band PSF in a 2×2 pixel array. In this way, the increased Strehl ratio in the H band provided by NFIRAOS is better exploited. Figure 7 shows the performance improvement of utilizing λ_H/d instead of λ_J/d pixels for a typical asterism (top panel) and as a function of the sky coverage (bottom panel). The RMS wavefront errors in the tip/tilt modes and full set of NGS modes at 50% sky coverage are reduced from 68.2/92.6 nm RMS to 62.6/87.8 nm RMS, or about 30 nm in quadrature.

E. Pixel Processing Algorithms

It was found that the constrained matched filter [21] previously developed for the LGS WFS does not provide optimal performance for the NGS WFS, probably due to the small image size and the very small number of pixels with nonnegligible SNR. The classical, unconstrained matched filter generally gives better results. Figure 8 shows a performance comparison between (1) the classical unconstrained matched filter, (2) the constrained matched filter for linearity over a full ± 1 pixel shift, and (3) a thresholded center of gravity method (with a 3σ threshold). The top panel shows results obtained with a "typical" asterism near median sky coverage. The bottom panel shows the wavefront error reduction of the classic unconstrained matched filter compared with the

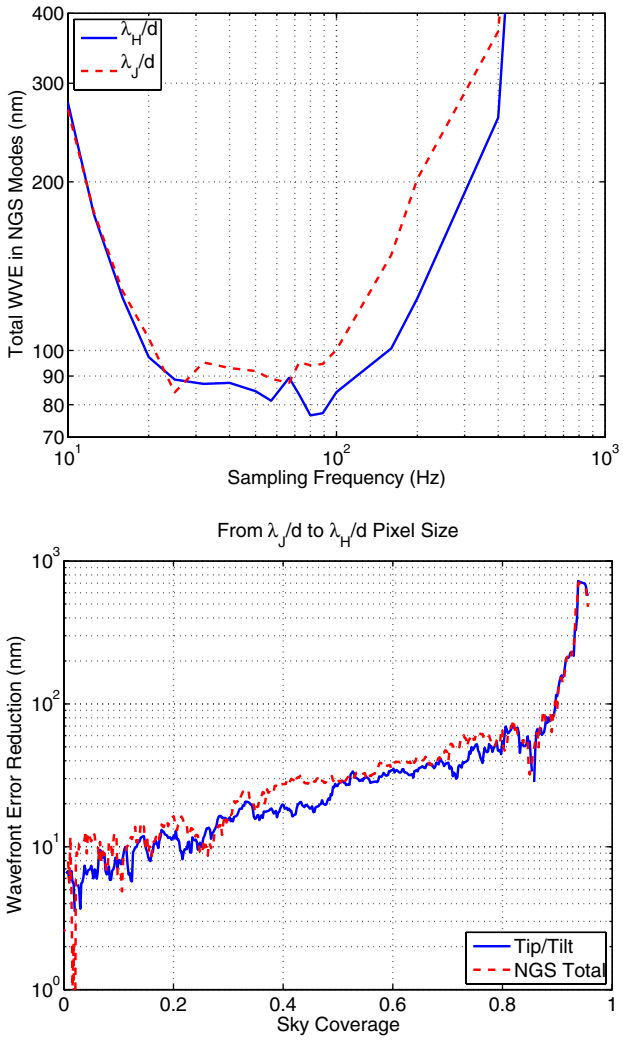

Fig. 7. (Color online) Reduction in wavefront error obtained by making detector pixel size λ_H/d instead of λ_J/d.

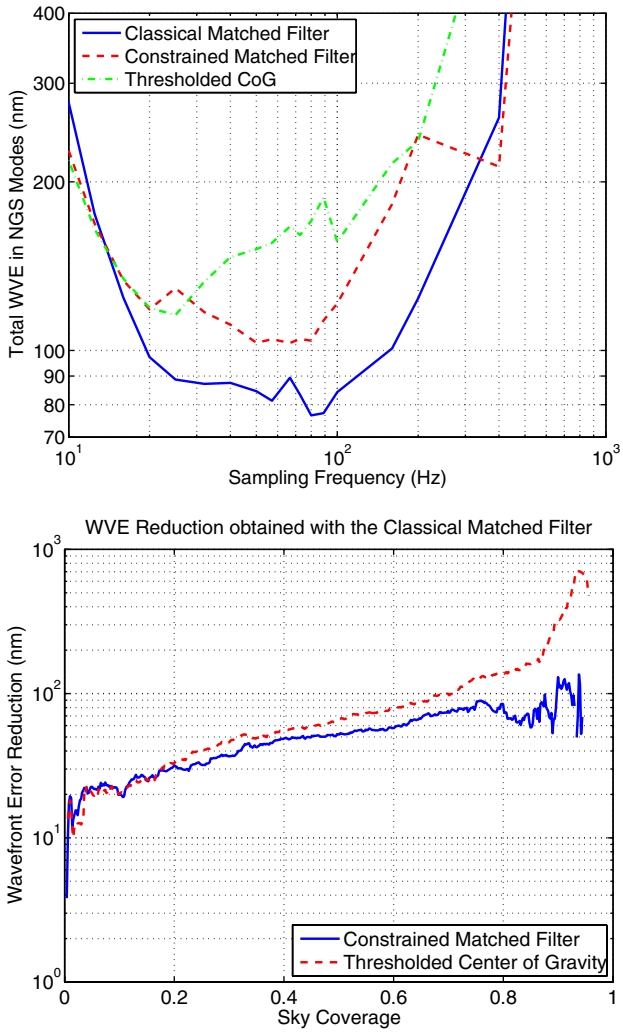

Fig. 8. (Color online) Comparison of different pixel processing algorithms.

constrained matched filter and the thresholded center of gravity as a function of the sky coverage. The classic, unconstrained matched filter gives much better results than either the center of gravity method or the constrained matched filter (about 50 to 70 nm RMS at 50% sky coverage).

F. "Demoting" the TTF WFS

It was found that for certain asterisms that include a brighter TTF NGS and dimmer TT NGSs, "demoting" the TTF WFS to a simple TT WFS by averaging the gradient measurements of the four subapertures generally gave better performance, and that this approach could reduce the tip/tilt error at median sky coverage by a significant amount. At the current stage, we are not completely sure about the reason behind this. The top panel in Fig. 9 shows the performance gain in the tip/tilt modes obtained by "demoting" the TTF NGS WFS for a sample asterism. The J band magnitude of the 3 NGS are 17.5, 19.8, and 20.0, respectively.

During sky coverage simulations, we "demote" TTF adaptively by running the simulation with and without "demoting" and then pick the option that gives smaller residual wavefront error. The bottom panel in Figure 9 shows the performance gain obtained for the sky coverage simulation. The tip/tilt wavefront error at median sky coverage is reduced by 54.8 nm RMS in quadrature.

6. Sky Coverage Results

We have validated the sky coverage postprocessing simulation against integrated LAOS simulations of both LGS and NGS mode control. We considered four symmetrical and asymmetrical asterisms with a range of NGS wavefront sensing options and found that by adjusting both the tip/tilt and quadratic modes of the NGS wavefront, the postprocessing method agrees very well with the integrated simulation, despite modest fluctuations in performance due to the coarse sampling of the NGS WFS pupil functions.

The baseline conditions for the NFIRAOS sky coverage simulations are median seeing and guide star statistics at the Galactic pole, which has the lowest star densities. Other conditions, such as 25% seeing

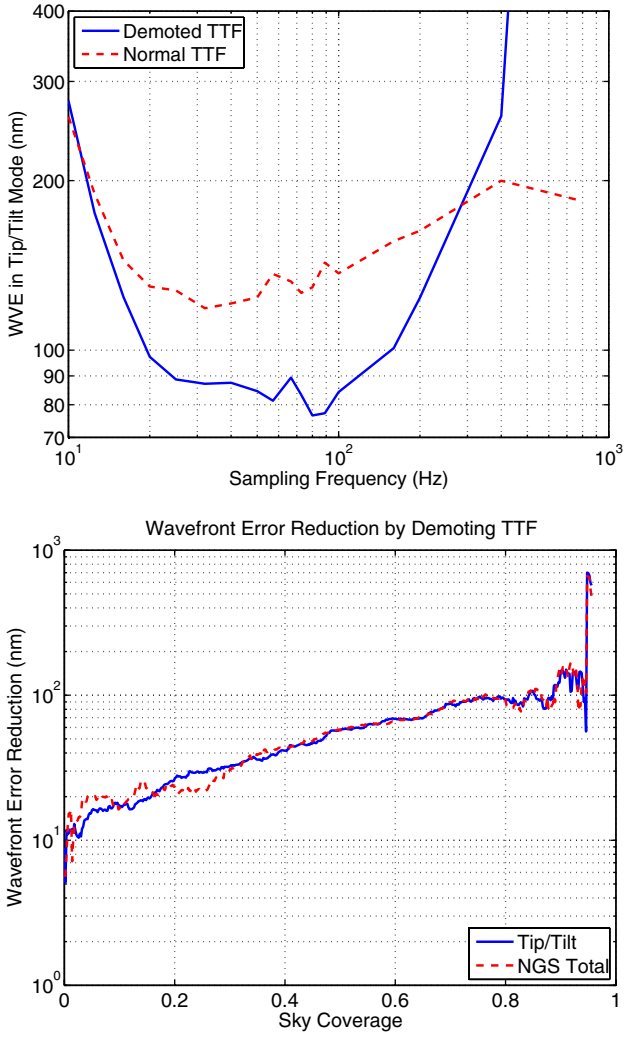

Fig. 9. (Color online) Top panel: The reduction in tip/tilt wavefront error obtained by demoting the TTF WFS for a sample asterism. Bottom panel: Improved tip/tilt compensation as a function of sky coverage obtained by selectively demoting the TTF WFS for the estimation of global tip/tilt modes. The change in the wavefront error for the plate scale modes is negligible. The J band magnitudes of the 3 NGSs are 17.5, 19.8, and 20.0, respectively.

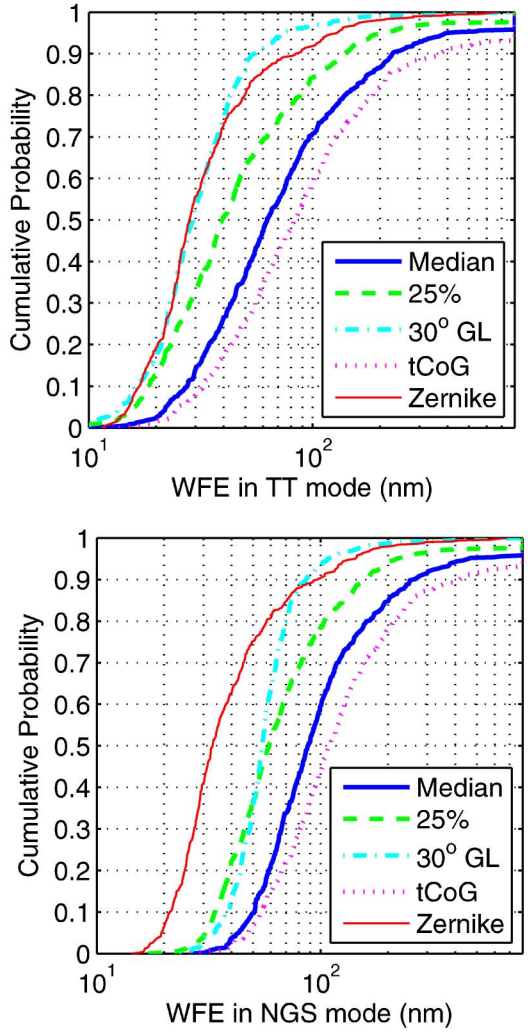

Fig. 10. (Color online) Sky coverage results for different conditions. The solid blue curves labeled as "Median" are sky coverage results for the nominal conditions of median seeing and guide star statistics at the Galactic pole. The dashed green curves labeled as "25%" are results under 25% seeing conditions. The dash-dot cyan curves labeled as "30° GL" are results for guide star statistics at 30° Galactic latitude. The dotted magenta curves labeled as "tCoG" are for the thresholded center of gravity pixel processing method instead of the matched filter. The red, thin curves labeled as "Zernike" are the results from the original Zernike-based geometric sky coverage simulation.

conditions and guide star statistics at 30° galactic latitude, are also studied to show the improvements obtained in better conditions. The wavefront error in the NGS modes refers to the error in both tip/tilt and plate scale modes. This is the total wavefront error introduced from imperfect NGS compensation that degrades the science image. It also includes the residual telescope wind shake in the tip/tilt modes and the additional sodium layer focus tracking error. Finally, the budgeted NFIRAOS wavefront implementation error of 103 nm RMS has been included in the simulation by reducing the NGS signal levels by the corresponding loss of Strehl in J and H bands.

Figure 10 shows the wavefront errors in the tip/tilt and the full set of NGS modes under various conditions. The solid blue and dashed green curves show the wavefront error as a function of sky coverage for median ($r_0 = 0.15$ m) and 25% ($r_0 = 0.26$ m) seeing conditions with the classical matched filter algorithm for the NGS WFS pixel processing. The median sky coverage wavefront errors in the tip/tilt and NGS modes are 62.6 nm and 87.8 nm RMS for median seeing conditions, and they improve to 39.4 nm and 59.0 nm RMS for 25% seeing conditions. The dash-dot cyan curves show the result for median seeing condition, but using guide star statistics at 30° north Galactic latitude, which has a much higher density of stars. The median sky coverage wavefront errors in the tip/tilt and the NGS modes are 29.1 and 54.8 nm RMS, which are again much improved from the Galactic pole.

Table 3. NFIRAOS NGS Mode Error Budget at Median Sky Coverage[a]

Error Source	Tip/Tilt	Plate Scale Modes	Total NGS Modes
Atmospheric turbulence	46.5	54.3	72.2
NGS WFS noise	39.0	21.1	47.7
Telescope wind shake	15.45	0	8.43
Na layer range tracking	0	0	12.38
Total	62.63	58.2	87.8

[a]The contributions from the atmospheric turbulence are obtained by running noise free simulations. Notice that the values in the tip/tilt and place scale mode columns do not precisely sum up (quadratically) to the values in the total NGS mode column because they are median, not mean, values.

The dotted magenta curves show the results for median seeing conditions at the Galactic pole, using a thresholded center of gravity method instead of the matched filter. The median sky coverage wavefront errors in the tip/tilt and the NGS modes are 82.9 nm and 110.2 nm RMS, which are increases of 54.3 nm and 66.6 nm (in quadrature) from the matched filter case.

The results from the original Zernike-based geometric sky coverage simulation of NFIRAOS [6,7] are shown in solid thin red curves for comparison. The wavefront error obtained in our simulations is larger than the results obtained in these Zernike-based geometric simulations. We attribute this degradation to a variety of reasons: (a) The NGS WFS noise model was too optimistic, (b) cross coupling from residual wavefront errors in LGS controlled modes into NGS WFS measurements was significant, and (c) the different choices of control algorithm (split versus integrated tomography).

Finally, an error budget breakdown for the case of median sky coverage at the Galactic pole is summarized in Table 3.

7. Summary and Future Work

We have described a high fidelity, computationally efficient, time domain sky coverage simulation for the TMT NFIRAOS system. The method can be readily expanded to model other multiconjugate or multiobject adaptive optics systems. A novel technique to model the impact of quadratic wavefront aberrations on PSFs is described, which is crucial for obtaining good agreement between the postprocessing and integrated simulations. The simulation has already proved valuable for optimizing a variety of control system parameters and algorithms, such as pixel size, matched filter pixel processing, type II control of the plate scale modes, and adaptively "demoting" the TTF WFS.

In Subsection 5.D we showed that sky coverage can be improved by increasing pixel size to match the size of the *H* band diffraction limited PSF. Our analysis is based upon the assumption that the NGS WFS spots can be centered on the intersection of 2×2 detector pixels in classical quad cell fashion. In the real NFIRAOS, subpixel offsetting of the null point may be required due to atmospheric dispersion and field distortions. In this case, a smaller pixel may be desired, and careful trade studies on the pixel size must be made. A possible solution to mitigate this problem may be to use a small-range tip/tilt mirror in the NGS WFS optical design to steer the null point back to the intersection of 2×2 pixels.

The impact of the residual aberration in the plate scale modes upon the science PSF resembles tip/tilt jitter more than higher order aberrations. The same modeling approach used to simulate the NGS PSF can be used to calculate the time-averaged science PSF and and its enclosed energy characteristics, based on time histories of the complex PSFs for the science target and the residual tip/tilt and plate scale modes.

This work is supported by the National Science Foundation (NSF) Science Technology Center for Adaptive Optics, managed by the University of California at Santa Cruz under cooperative agreement AST-9876783.

This work is also supported by the Thirty Meter Telescope (TMT) project. The authors gratefully acknowledge the support of the TMT partner institutions. They are the Association of Canadian Universities for Research in Astronomy (ACURA), the California Institute of Technology, and the University of California. This work was supported as well by the Gordon and Betty Moore Foundation, the Canada Foundation for Innovation, the Ontario Ministry of Research and Innovation, the National Research Council of Canada, the Natural Sciences and Engineering Research Council of Canada, the British Columbia Knowledge Development Fund, the Association of Universities for Research in Astronomy (AURA), and the U.S. National Science Foundation.

References

1. P. L. Wizinowich, D. Le Mignant, A. H. Bouchez, R. D. Campbell, J. C. Y. Chin, A. R. Contos, M. A. van Dam, S. K. Hartman, E. M. Johansson, R. E. Lafon, H. Lewis, P. J. Stomski, D. M. Summers, C. G. Brown, P. M. Danforth, C. E. Max, and D. M. Pennington, "The W. M. Keck Observatory laser guide star adaptive optics system: overview," Publ. Astron. Soc. Pac. **118**, 297–309 (2006).
2. M. Boccas, F. Rigaut, M. Bec, B. Irarrazaval, E. James, A. Ebbers, C. d'Orgeville, K. Grace, G. Arriagada, S. Karewicz, M. Sheehan, J. White, and S. Chan, "Laser guide star upgrade of Altair at Gemini North," Proc. SPIE **6272**, 62723L (2006).
3. M. Le Louarn, N. N. Hubin, and R. Arsenault, "Adaptive optics for second-generation VLT instruments," Proc. SPIE **5490**, 248–259 (2004) .
4. B. Ellerbroek, S. Adkins, D. Andersen, J. Atwood, C. Boyer, P. Byrnes, R. Conan, L. Gilles, G. Herriot, P. Hickson, E. Hileman, D. Joyce, B. Leckie, M. Liang, T. Pfrommer, J.-C. Sinquin, J.-P. Veran, L. Wang, and P. Welle, "Progress toward developing the TMT adaptive optical systems and their components," Proc. SPIE **7015**, 70150R (2008).

5. E. Diolaiti, J.-M. Conan, I. Foppiani, M. Lombini, C. Petit, C. Robert, L. Schreiber, P. Ciliegi, E. Marchetti, M. Bellazzini, L. Busoni, S. Esposito, T. Fusco, N. Hubin, F. Quiros-Pacheco, A. Baruffolo, S. D'Odorico, J. Farinato, B. Neichel, R. Ragazzoni, C. Arcidiacono, V. Biliotti, G. Bregoli, G. Cosentino, and G. Innocenti, "A preliminary overview of the multiconjugate adaptive optics module for the E-ELT," Proc. SPIE **7015**, 70150U (2008).
6. R. M. Clare, B. L. Ellerbroek, G. Herriot, and J.-P. Véran, "Adaptive optics sky coverage modeling for extremely large telescopes," Appl. Opt. **45**, 8964–8978 (2006).
7. R. M. Clare and B. L. Ellerbroek, "Sky coverage estimates for adaptive optics systems from computations in Zernike space," J. Opt. Soc. Am. A **23**, 418–426 (2006).
8. B. Ellerbroek, "A high fidelity, physical optics sky coverage simulation tool for laser guide star multi-conjugate and multi-object ao systems," CFAO Proposal (2008). [Available upon request]
9. J.-P. Veran and G. Herriot, "Type II woofer-tweeter control for NFIRAOS on TMT," in OSA Technical Digest (CD) (Optical Society of America, to be published).
10. L. Gilles and B. L. Ellerbroek, "Split atmospheric tomography using laser and natural guide stars," J. Opt. Soc. Am. A **25**, 2427–2435 (2008).
11. B. L. Ellerbroek and F. Rigaut, "Methods for correcting tilt anisoplanatism in laser-guide-star-based multiconjugate adaptive optics," J. Opt. Soc. Am. A **18**, 2539–2547 (2001).
12. B. L. Ellerbroek, "Efficient computation of minimum-variance wave-front reconstructors with sparse matrix techniques," J. Opt. Soc. Am. A **19**, 1803–1816 (2002).
13. L. Gilles, B. Ellerbroek, and J.-P. Véran, "Laser guide star multi-conjugate adaptive optics performance of the Thirty Meter Telescope with elongated beacons and matched filtering," Proc. SPIE **6272**, 627236 (2006).
14. J. Vernin, A. Agabi, R. Avila, M. Azouit, R. Conon, F. Martin, E. Masciadri, L. Sanchez, and A. Ziad, "1998 Gemini site testing campaign: Cerro Panchon and Cerro Tololo," Gemini Document RTP-AO-G0094 (Gemini Observatory, 2000).
15. A. C. Robin, C. Reylé, S. Derrière, and S. Picaud, "A synthetic view on structure and evolution of the Milky Way," Astron. Astrophys. **409**, 523–540 (2003).
16. http://model.obs-besancon.fr/.
17. C. Willott, Univeristy of Ottawa, Department of Physics, 150 Louis Pasteur, MacDonald Hall, Ottawa Ontario K1N 6N5, Canada.
18. D. Andersen, NRC HIA, 5071 West Saanich Road, Victoria, British Columbia V9E 2E7, Canada.
19. G. Herriot, P. Hickson, B. Ellerbroek, J.-P. Véran, C.-Y. She, R. Clare, and D. Looze, "Focus errors from tracking sodium layer altitude variations with laser guide star adaptive optics for the Thirty Meter Telescope," Proc. SPIE **6272**, 62721I (2006).
20. L. Gilles and B. Ellerbroek, "Shack-Hartmann wavefront sensing with elongated sodium laser beacons: centroiding versus matched filtering," Appl. Opt. **45**, 6568–6576 (2006).
21. L. Gilles and B. L. Ellerbroek, "Constrained matched filtering for extended dynamic range and improved noise rejection for Shack-Hartmann wavefront sensing," Opt. Lett. **33**, 1159–1161 (2008).
22. J.-P. Véran and G. Herriot, "Woofer-tweeter tip-tilt control for NFIRAOS on TMT," Proc. SPIE **6272** 62721R (2006).
23. M. S. Bessell and J. M. Brett, "JHKLM photometry: standard systems, passbands, and intrinsic colors," Pub. Astron. Soc. Pac. **100**, 1134–1151 (1988).